Electronic Supplementary Material (ESI) for Photochemical & Photobiological Sciences.

Supporting Information

A new Schiff-based chemosensor for selective detection of Cu^{2+} and Co^{2+} and its copper complex for colorimetric sensing of S^{2-} in aqueous solution

Min Seon Kim, Seong Youl Lee, Jae Min Jung, Cheal Kim*

Department of Fine Chemistry and Department of Interdisciplinary Bio IT Materials, Seoul National University of Science and Technology, Seoul 139-743, Republic of Korea. Fax: +82-2-973-9149; Tel: +82-2-970-6693; E-mail: chealkim@seoultech.ac.kr

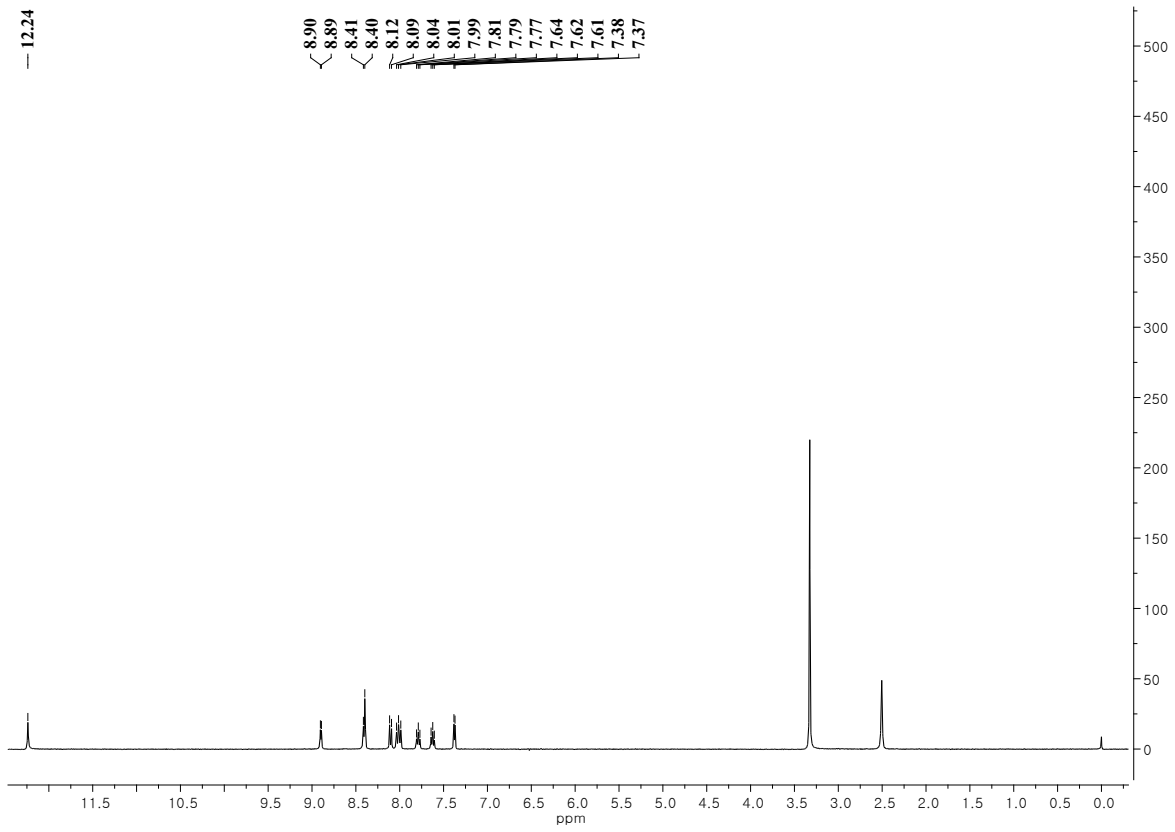

Fig. S1 ^{1}H NMR spectrum of **1**.

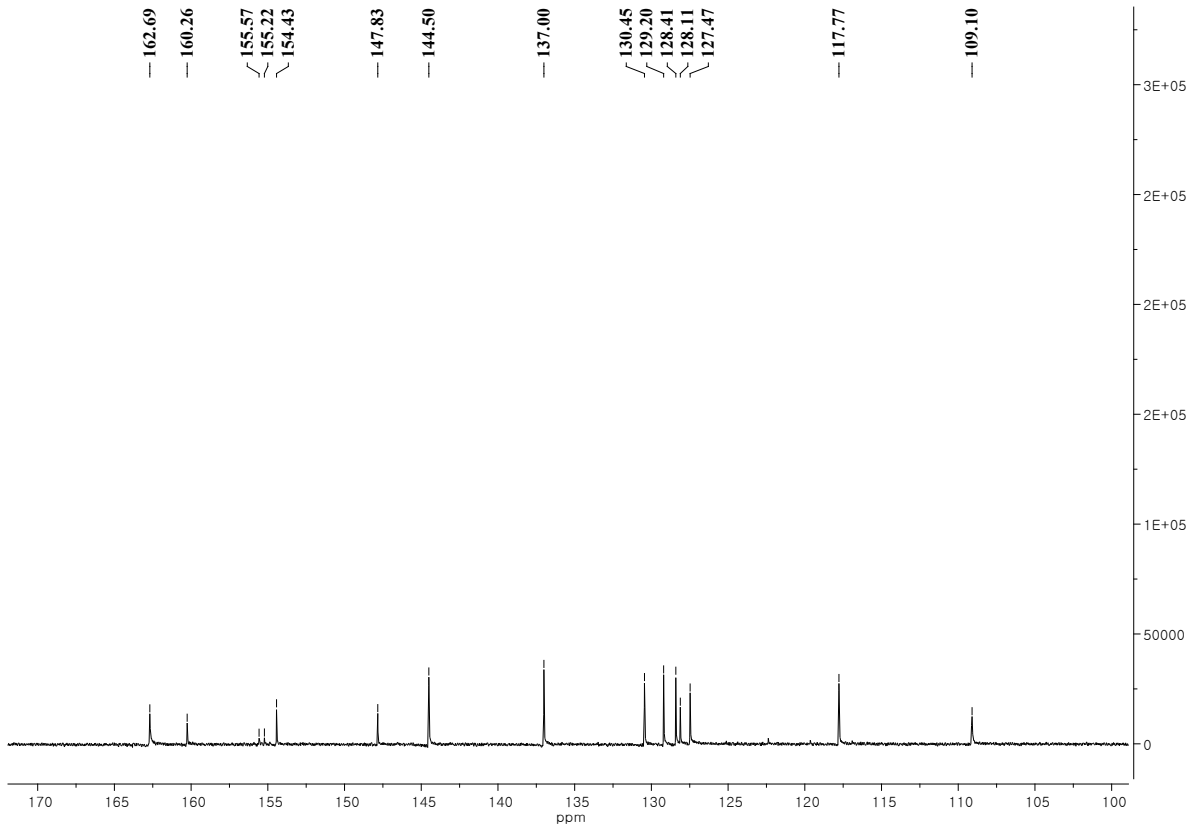

Fig. S2 ^{13}C NMR spectrum of **1**.

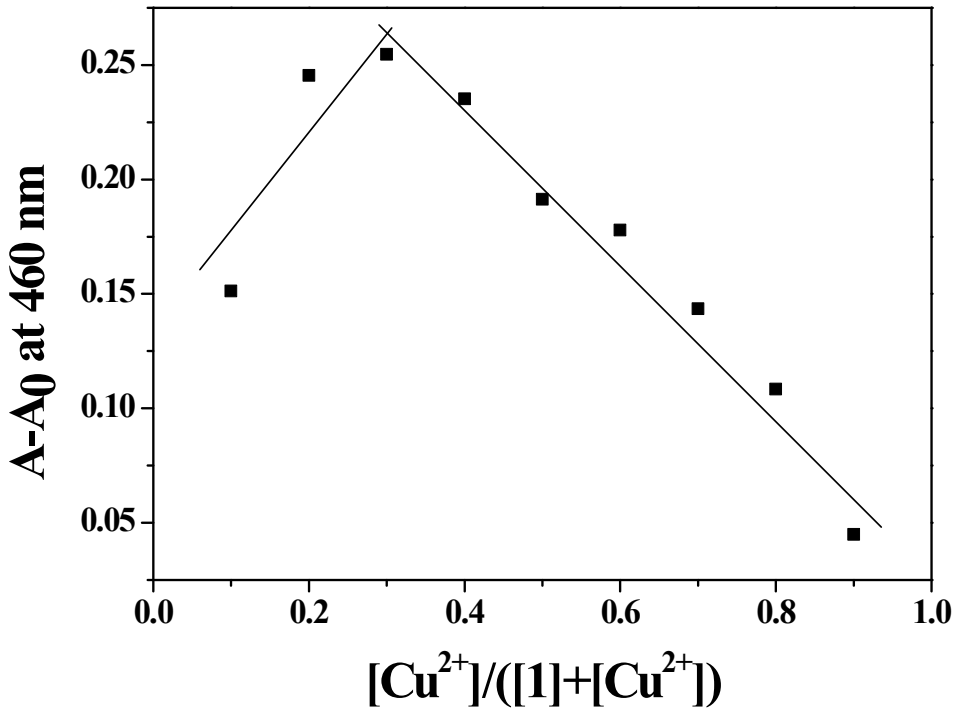

Fig. S3 Job's plot for the binding of **1** with Cu^{2+}. Absorbance at 460 nm was plotted as a function of the molar ratio of $[Cu^{2+}]/([\mathbf{1}]+[Cu^{2+}])$. The total concentration of Cu^{2+} ions with receptor **1** was 5.0×10^{-5} M.

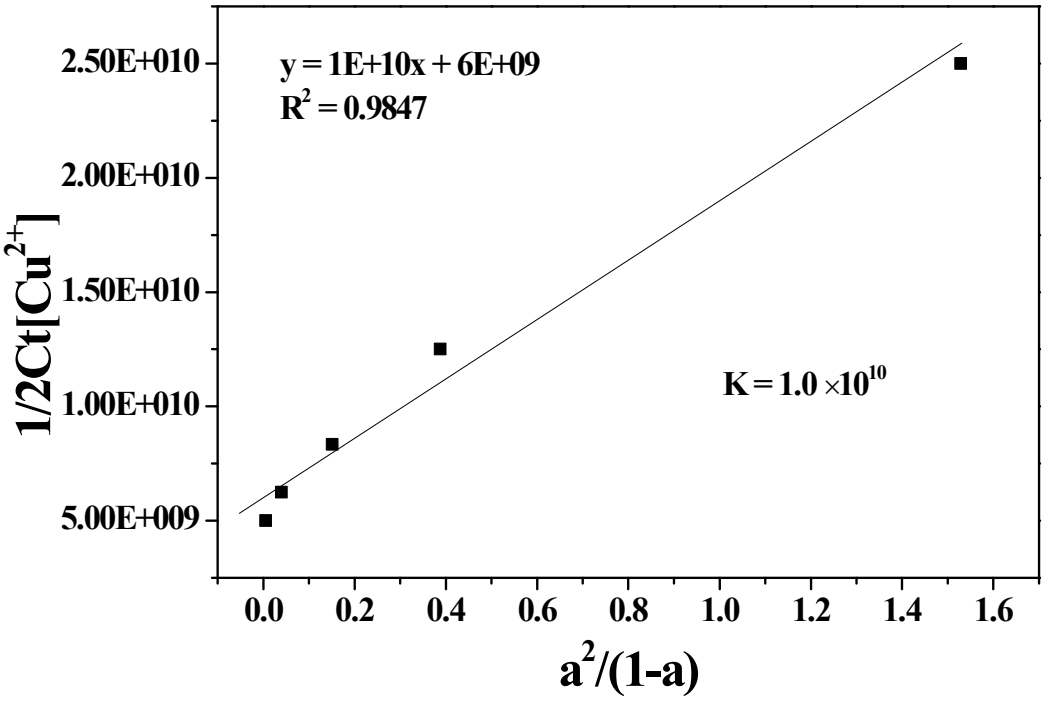

Fig. S4 Li's plot (at 460 nm) of **1** (10 μM), assuming 2:1 stoichiometry for association between **1** and Cu^{2+}.

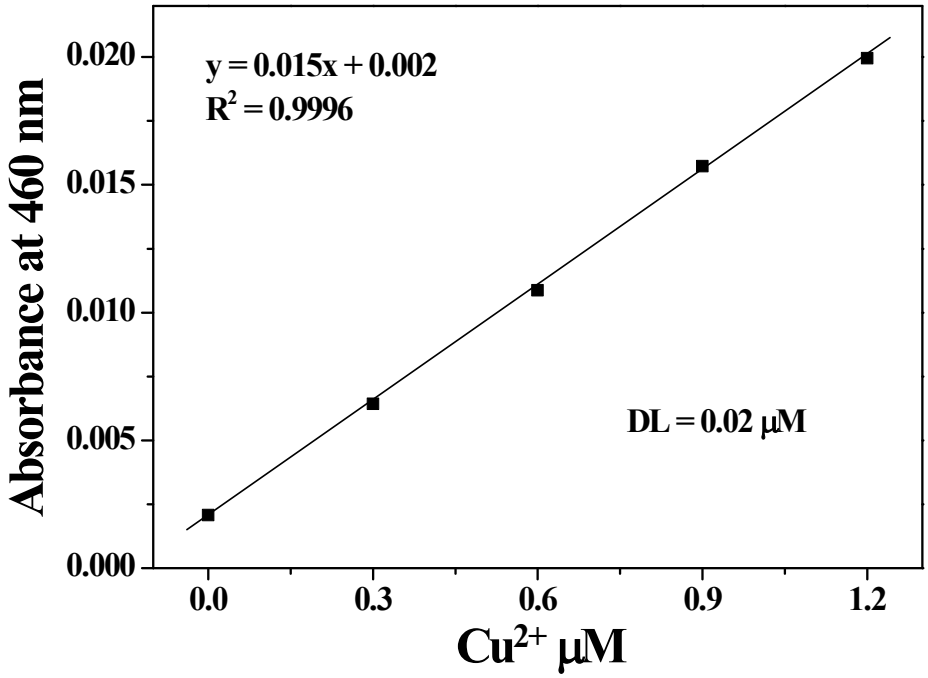

Fig. S5 Determination of the detection limit of **1** (10 μM) for Cu^{2+} based on change of absorbance at 460 nm.

(a)

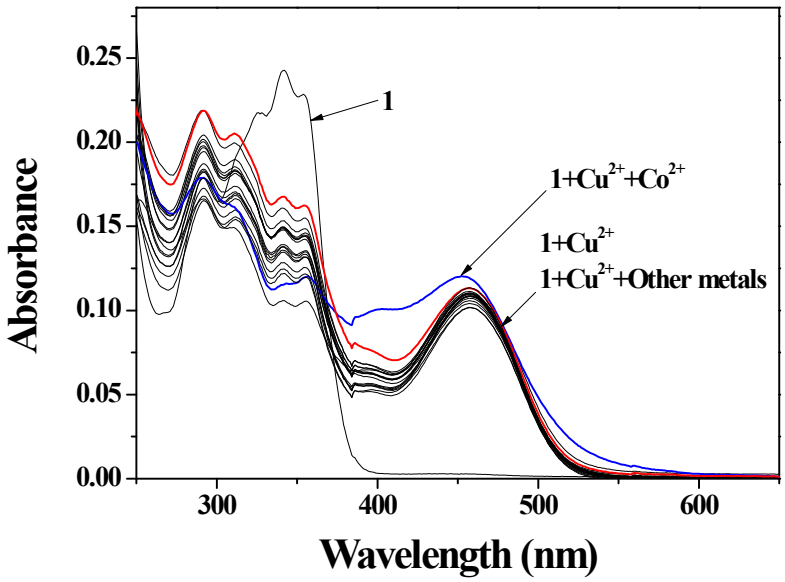

(b)

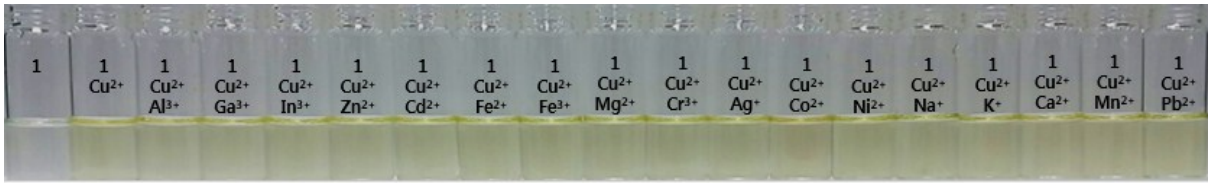

Fig. S6 (a) Absorption spectral changes of **1** (10 μM) upon addition of Cu^{2+} (1 equiv) in the absence and presence of 1 equiv of various metal ions in buffer/DMF solution (4:1; v/v, 10 mM bis-tris, pH 7.0). (b) The color changes of **1** (10 μM) upon addition of Cu^{2+} (1 equiv) in the absence and presence of 1 equiv of various metal ions in buffer/DMF solution (4:1; v/v, 10 mM bis-tris, pH 7.0).

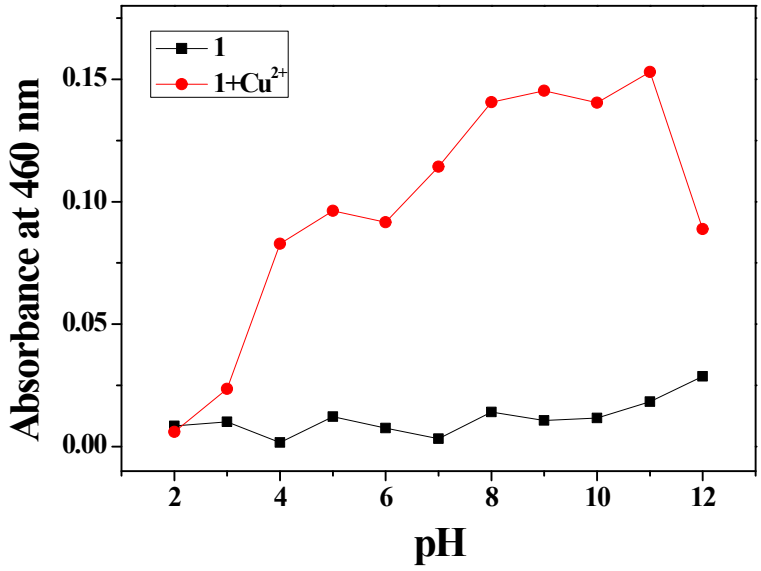

Fig. S7 UV-vis absobance (at 460 nm) of **1** and Cu^{2+}-2·**1** complex at different pH values (2-12).

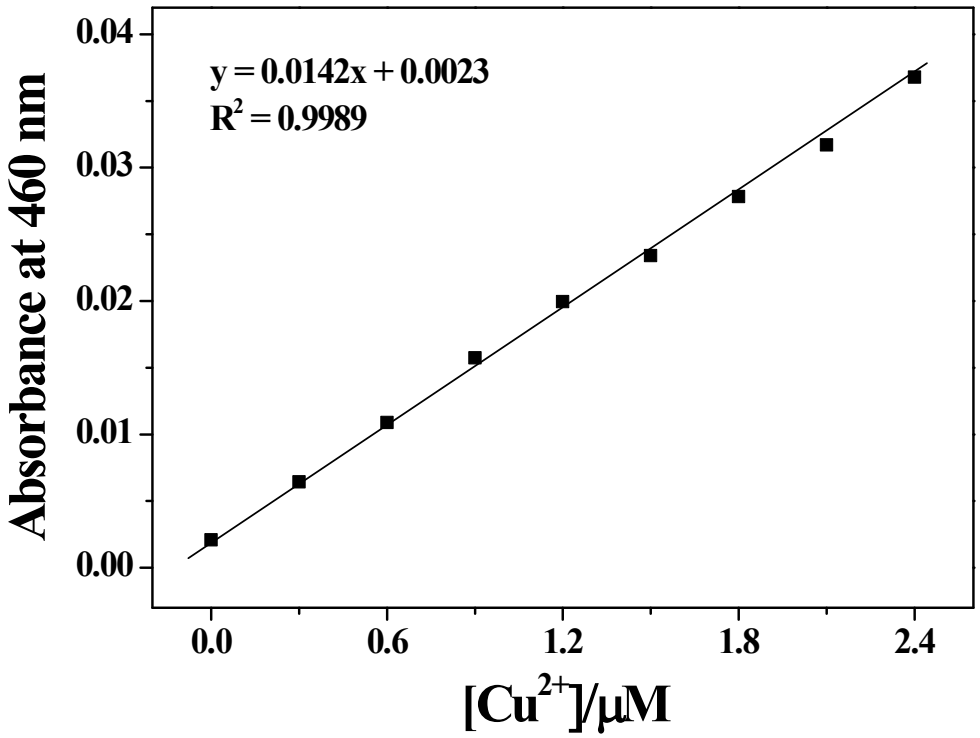

Fig. S8 Absorbance (at 460 nm) of **1** as a function of Cu(II) concentration ([**1**] = 10 μmol/L and [Cu(II)] = 0.0-2.4 μmol/L). Conditions: all samples were conducted in bis-tris buffer/DMF (4:1; v/v).

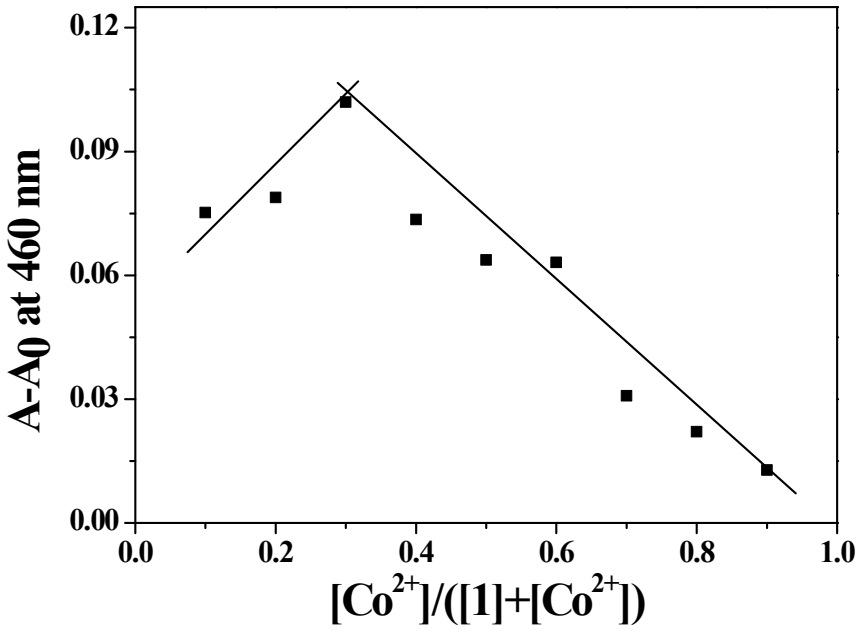

Fig. S9 Job's plot for the binding of **1** with Cu^{2+}. Absorbance at 460 nm was plotted as a function of the molar ratio of $[Co^{2+}]/([\mathbf{1}]+[Co^{2+}])$. The total concentration of Co^{2+} ions with receptor **1** was 1.0 x 10^{-5} M.

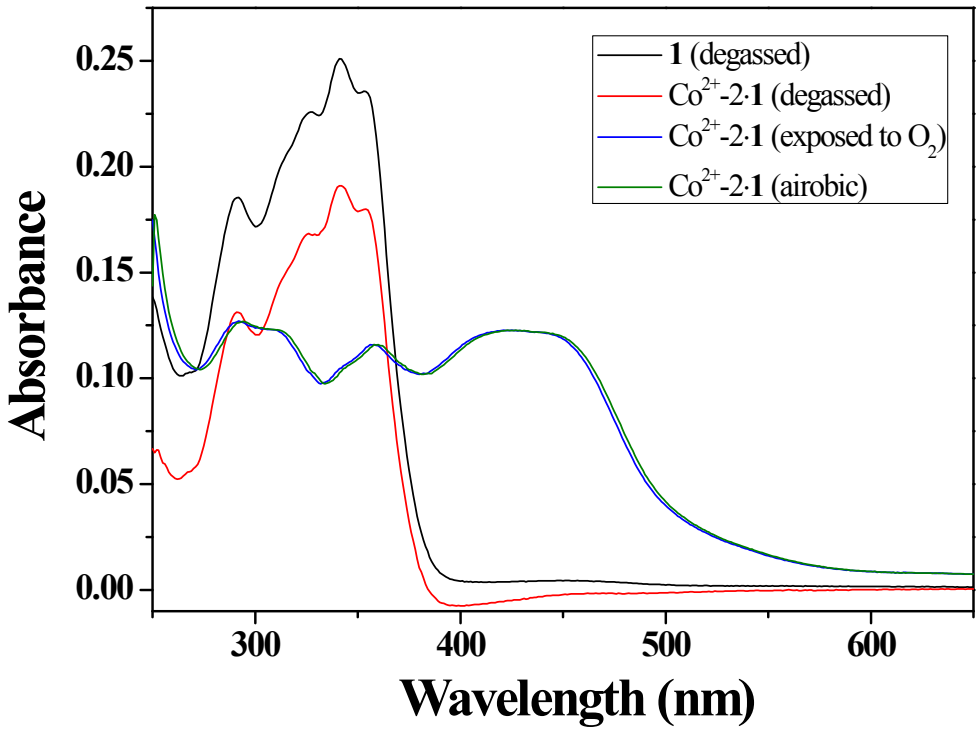

Fig. S10 Absorption spectra of **1** (10 μM), Co^{2+}-2·**1** complex under the degassed and exposure-to-air conditions, and Co^{2+}-2·**1** complex under aerobic conditions, respectively.

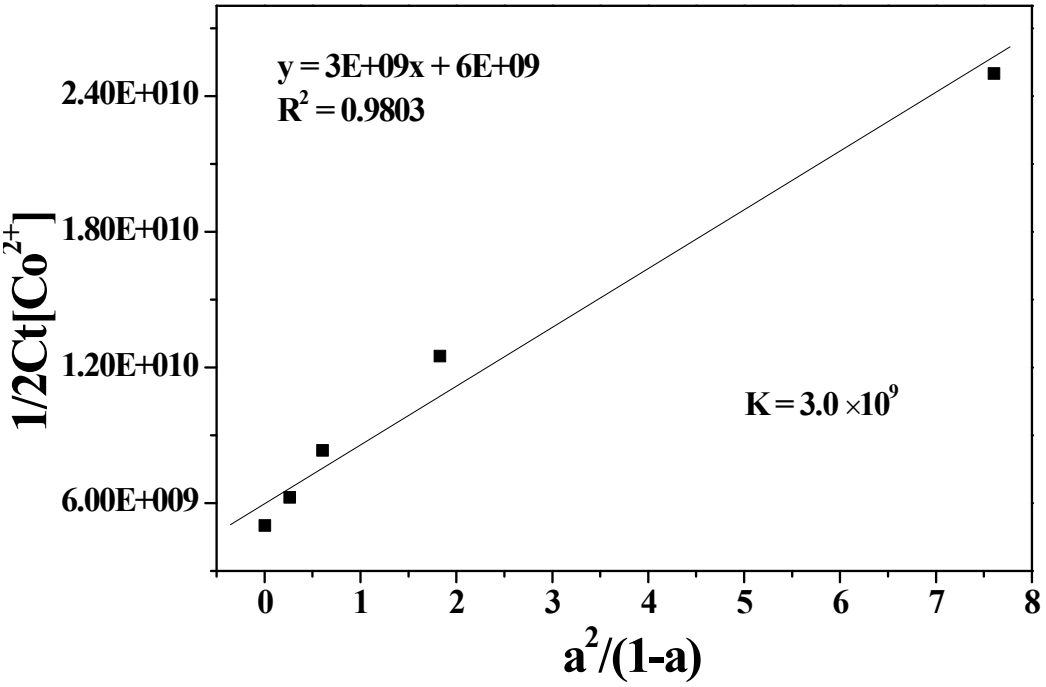

Fig. S11 Li's plot (at 460 nm) of **1** (10 μM), assuming 2:1 stoichiometry for association between **1** and Co^{2+}.

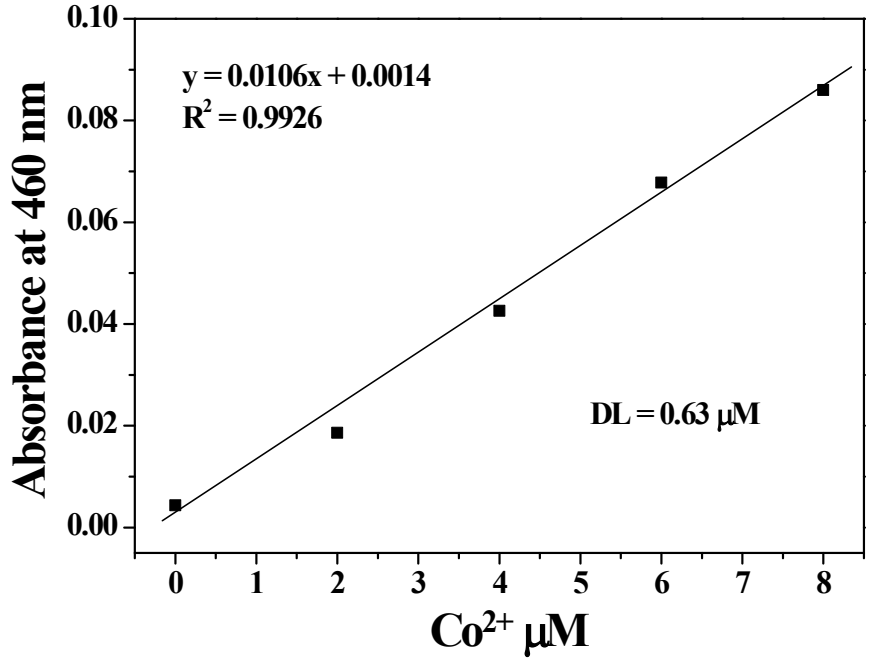

Fig. S12 Determination of the detection limit of **1** (10 μM) for Co^{2+} based on change of absorbance at 460 nm.

(a)

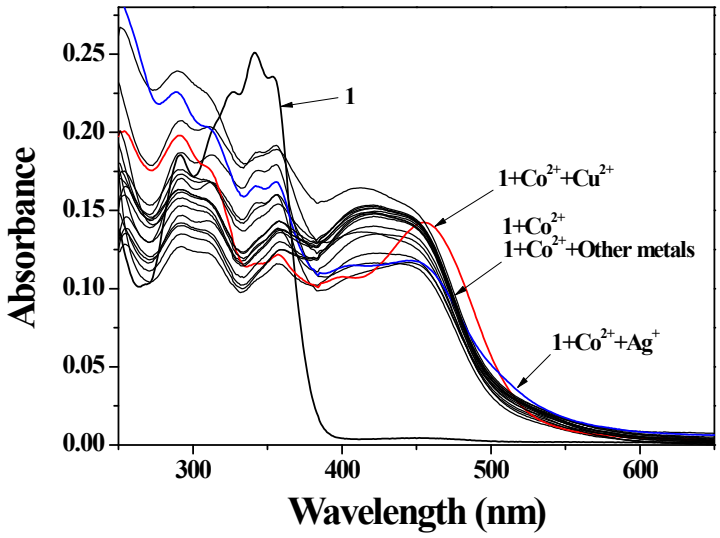

(b)

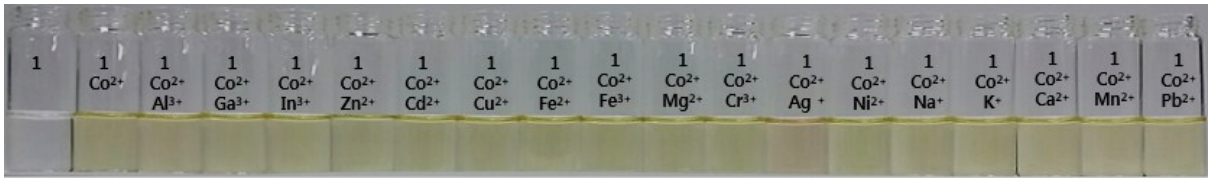

Fig. S13 (a) Absorption spectral changes of **1** (10 μM) upon addition of Co^{2+} (1.8 equiv) in the absence and presence of 1.8 equiv of various metal ions in buffer/DMF solution (4:1; v/v, 10 mM bis-tris, pH 7.0). (b) The color changes of **1** (10 μM) upon addition of Co^{2+} (1.8 equiv) in the absence and presence of 1.8 equiv of various metal ions in buffer/DMF solution (4:1; v/v, 10 mM bis-tris, pH 7.0).

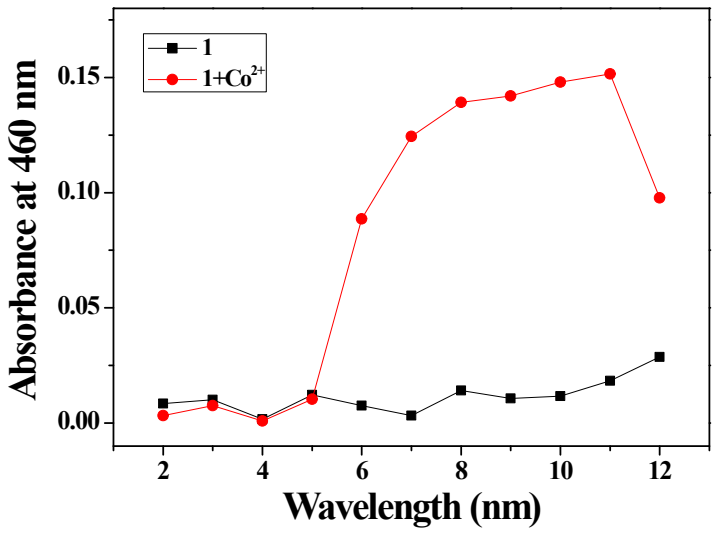

Fig. S14 UV-vis absorbance (at 460 nm) of **1** and Co^{2+}-2·**1** complex at different pH values (2-12).

(a)

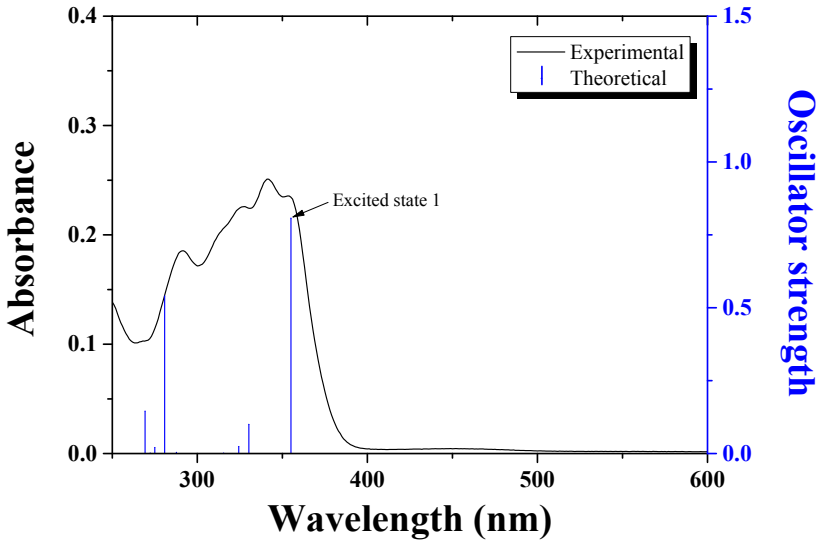

(b)

Excited state 1	Wavelength (nm)	Percent (%)	Main character	Oscillator strength
H → L	355.03	97	π → π*	0.8072

Fig. S15 (a) The theoretical excitation energies and the experimental UV-vis spectrum of **1**. (b) The major electronic transition energies and molecular orbital contributions for **1** (H = HOMO and L = LUMO).

(a)

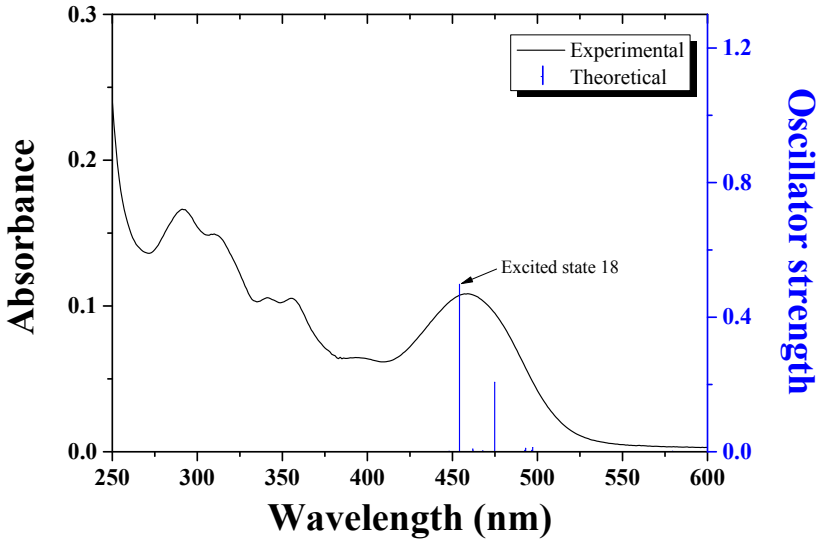

(b)

Excited state 18	Wavelength (nm)	Percent (%)	Main character	Oscillator strength
H - 1 (β) → L + 1 (β)	454.17	31	ICT	0.4974
H - 1 (α) → L (α)		29	ICT	
H (β) → L + 2 (β)		17	ICT	
H (α) → L + 1 (α)		16	ICT	

Fig. S16 (a) The theoretical excitation energies and the experimental UV-vis spectrum of Cu^{2+}-2·**1**. (b) The major electronic transition energies and molecular orbital contributions for Cu^{2+}-2·**1** (H = HOMO and L = LUMO).

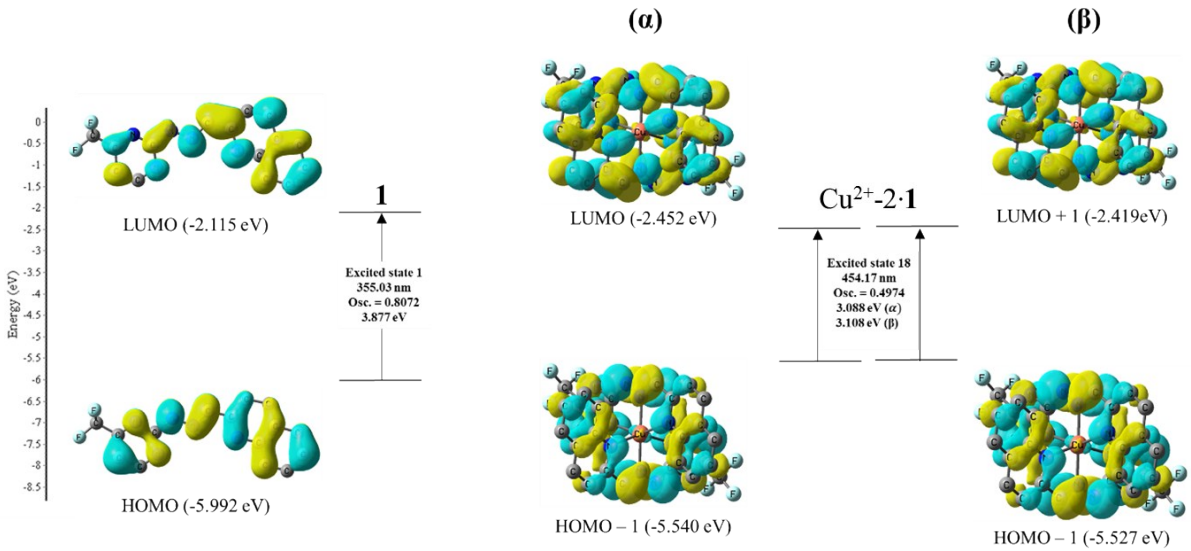

Fig. S17 Molecular orbital diagrams and excitation energies of **1** and Cu^{2+}-2·**1**.

(a)

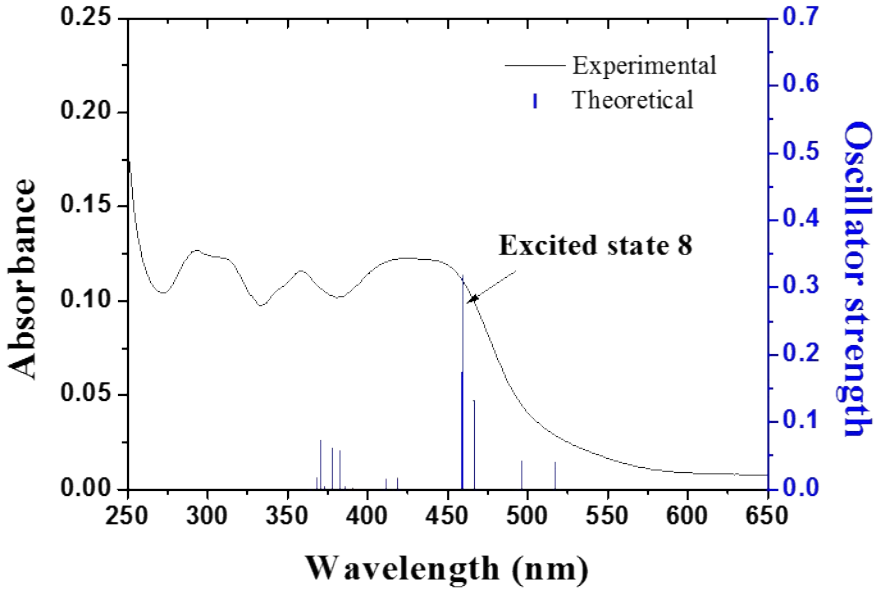

(b)

Excited state 8	Wavelength (nm)	Percent (%)	Main charcter	Oscillator strength
H-1 → L+1	459.8	56 %	ICT	0.3189
H-1 → L+3		20 %	LMCT	
H → L+2		19 %	ICT	

Fig. S18 (a) The theoretical excitation energies and the experimental UV-vis spectrum of Co^{3+}-2·**1**. (b) The major electronic transition energies and molecular orbital contributions for Co^{3+}-2·**1** (H = HOMO and L = LUMO).

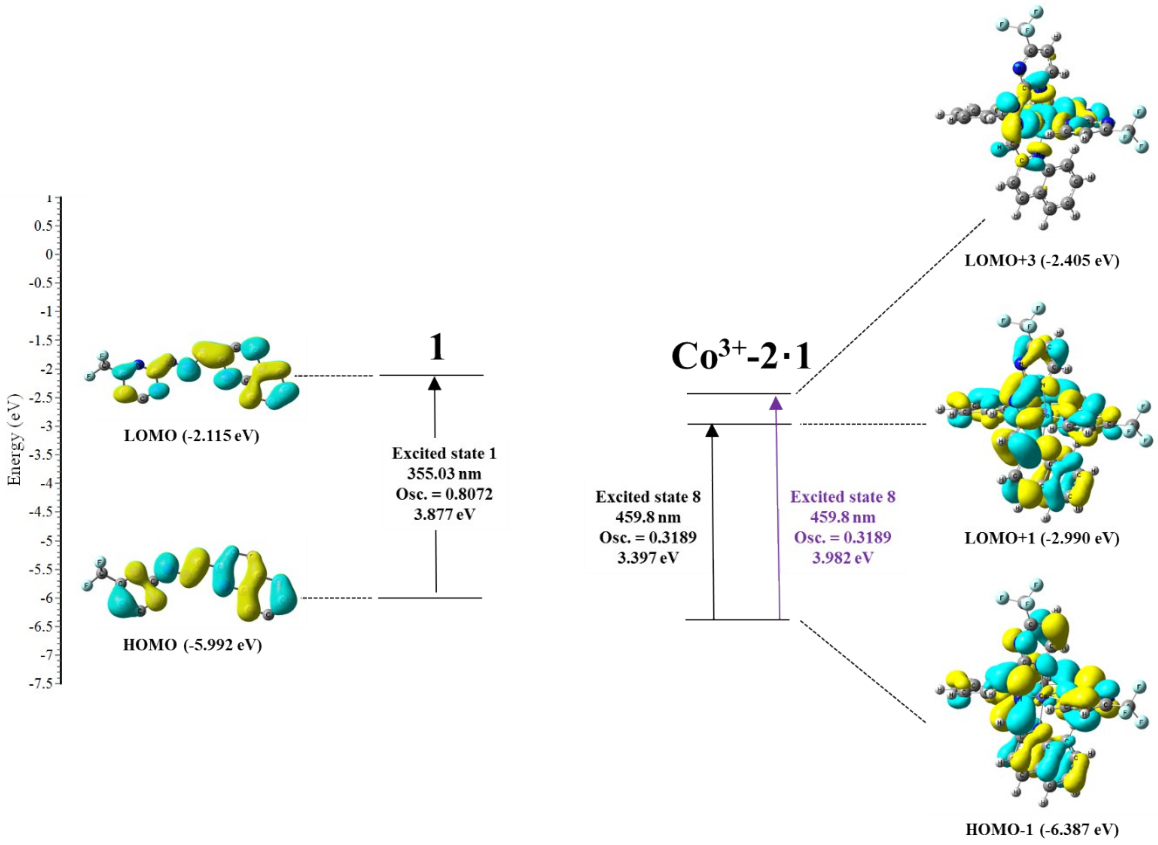

Fig. S19 Molecular orbital diagrams and excitation energies of **1** and Co^{3+}-2·**1**.

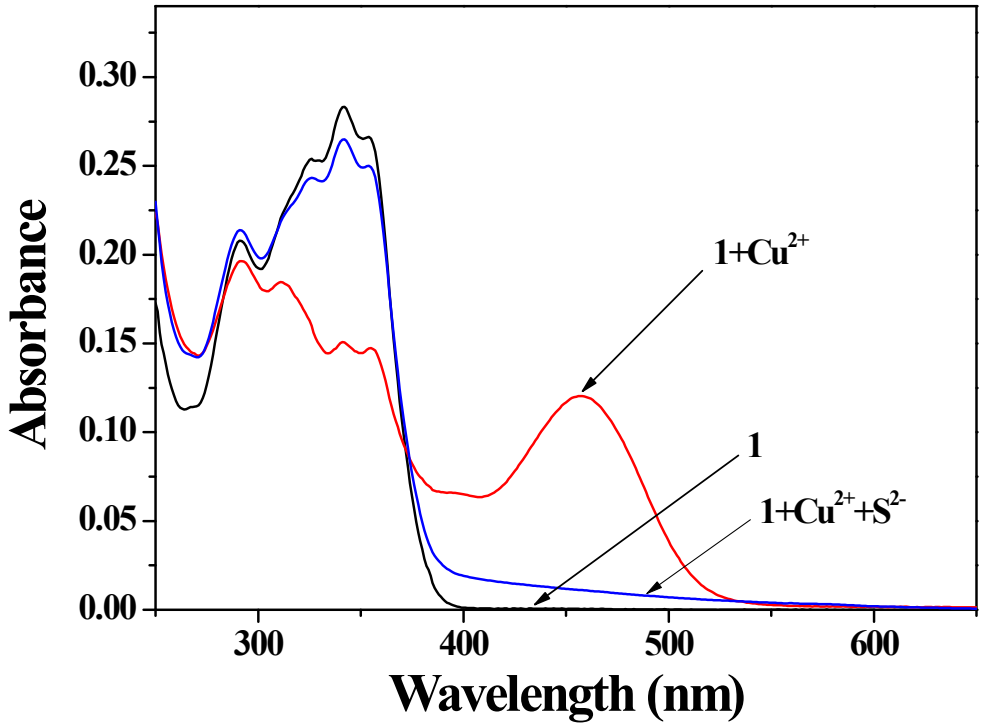

Fig. S20 UV-vis spectra of **1** (10 μM), Cu^{2+}-2·**1** (10 μM), and Cu^{2+}-2·**1** (10 μM) + S^{2-} (1.7 equiv) in buffer/DMF (4:1; v/v, 10 mM bis-tris, pH = 7.0).

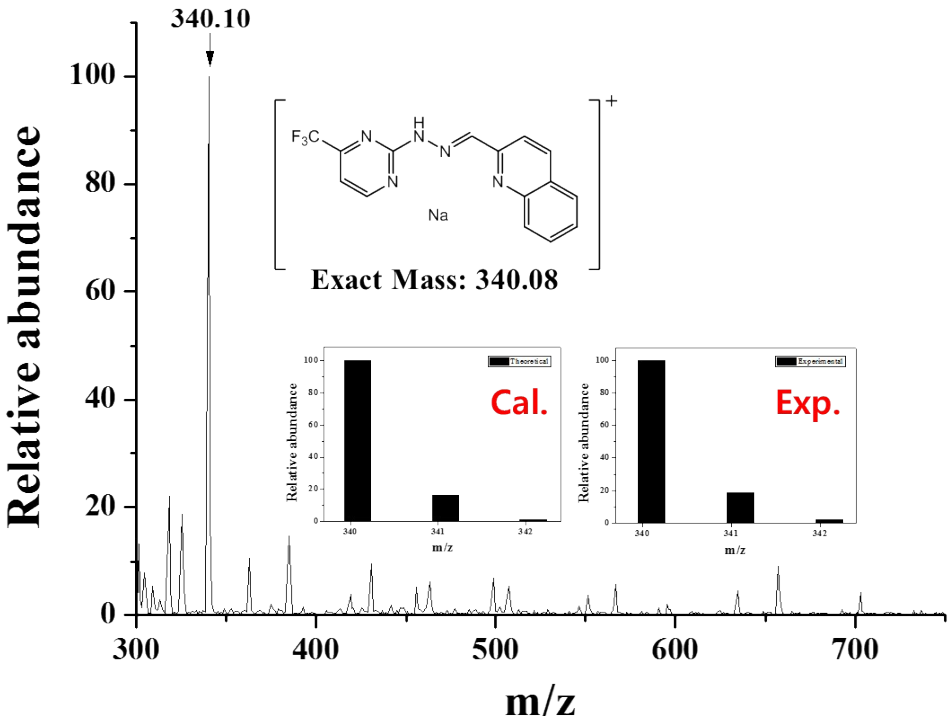

Fig. S21 Positive-ion electrospray ionization mass spectrum of Cu^{2+}-2·**1** (0.1 mM) upon addition of 1 equiv of S^{2-}.

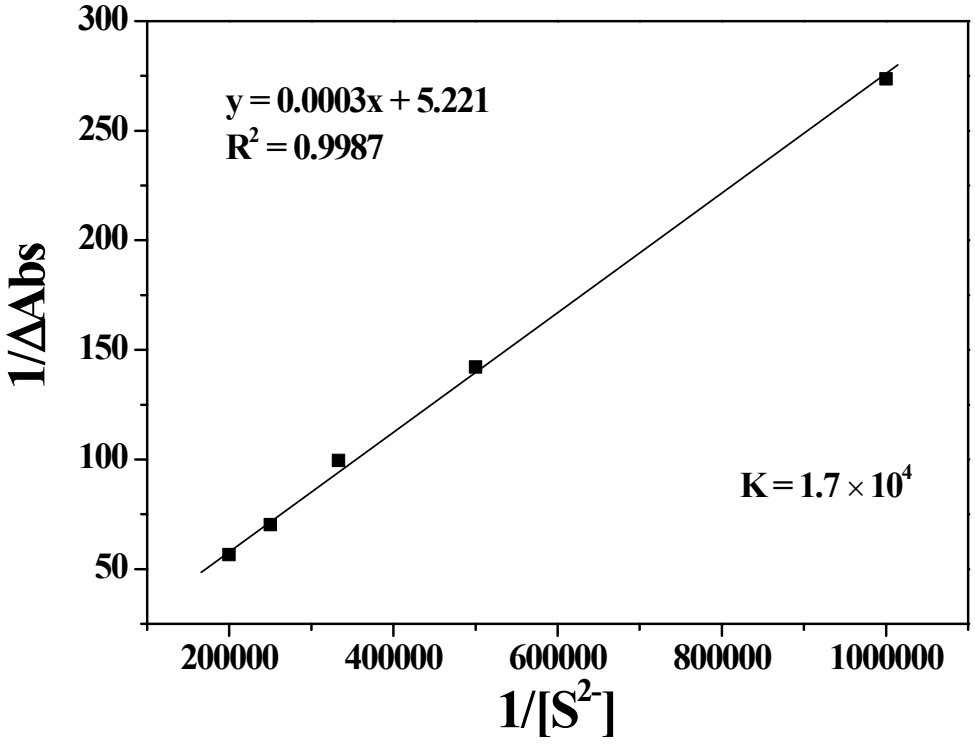

Fig. S22 Benesi-Hildebrand plot (at 460 nm) of Cu^{2+}-2·**1** (10 μM), assuming 1:1 stoichiometry for association between Cu^{2+}-2·**1** and S^{2-}.

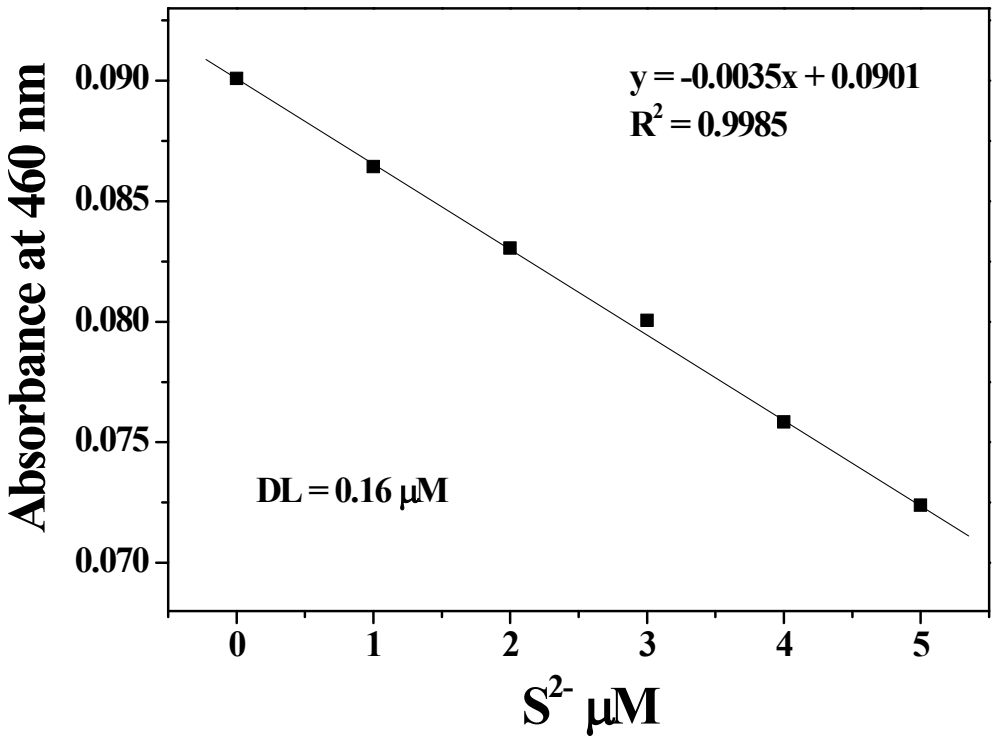

Fig. S23 Determination of the detection limit of Cu^{2+}-2·**1** (10 μM) for S^{2-} based on change of absorbance at 460 nm.

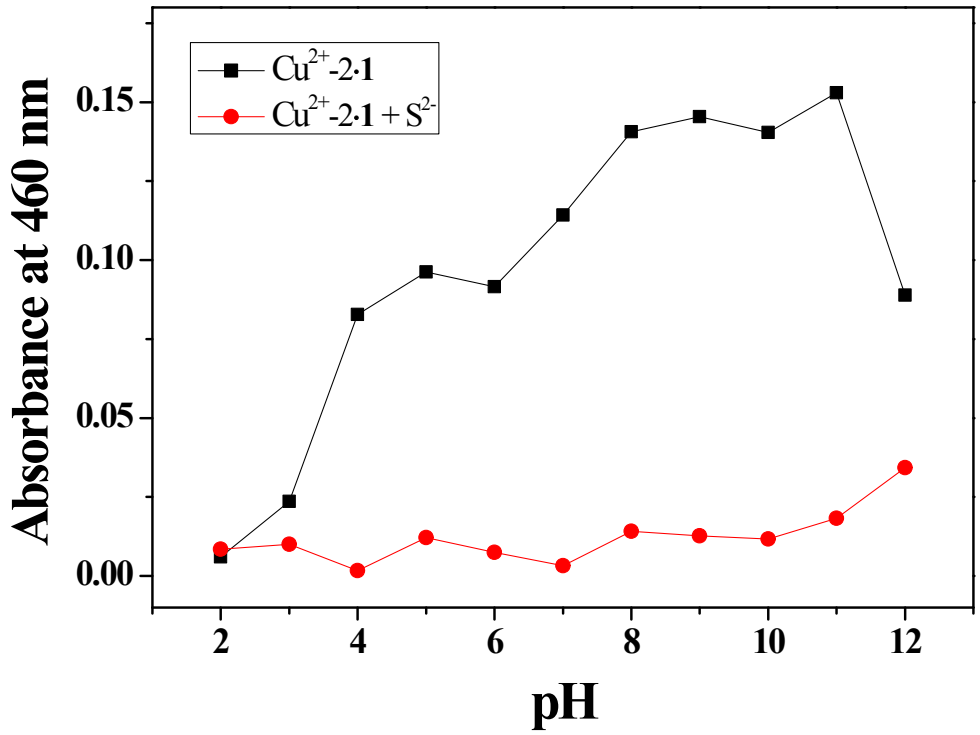

Fig. S24 UV-vis absorbance (at 460 nm) of Cu^{2+}-2·**1** and Cu^{2+}-2·**1** + S^{2-} at different pH values (2-12).